Digital Signal Processing 117 (2021) 103137

Contents lists available at ScienceDirect

Digital Signal Processing

www.elsevier.com/locate/dsp

fMRI activations via low-complexity second-order inverse-sparse-transform blind separation

Haifeng Wu *, Dong Li, Mingzhi Lu, Yu Zeng

School of Electrical & Information Technology, Yunnan Minzu University, Yunnan Provence, China

ARTICLE INFO

Article history:
Available online 11 June 2021

Keywords:
fMRI
BSS
SOBI
Inverse-sparse transform

ABSTRACT

Since functional Magnetic Resonance Imaging (fMRI) signals are a group of sparse signals, and its autocorrelation matrix contains limited information, it is difficult to accurately locate the brain activation area directly using traditional blind separation algorithms. For the issue, this paper proposes a method with inverse-sparse transform and second order blind identification (SOBI) for the separation of the activations. The contribution of this paper is to achieve the separation of sparse brain map signals and have lower computational complexity than higher-order statistical BSS. In experiments, we use both simulated and measured fMRI data to evaluate our method. The experimental results show that the proposed method's running time is only 1/30 of a higher-order statistical independent component analysis (ICA) algorithm, while its separation errors is close to ICA and less than half of a traditional SOBI algorithm.

1. Introduction

Functional Magnetic Resonance Imaging (fMRI) has been widely used in disease diagnosis and brain science research owing to its non-radiation and non-trauma, higher spatial resolution and signal-to-noise ratio than Electroencephalogram (EEG) and Magnetoencephalography (MEG). In the cortex area of brain activity, the relative decrease of deoxygenated hemoglobin concentration will lead to the enhancement of local magnetic field unevenness of blood vessels and peripheral tissues [1]. From this, fMRI can detect Blood Oxygenation Level Dependent (BOLD) in a subject's brain area. Collecting fMRI data requires designing experimental tasks first. When the subject performs a given task, the BOLD signal in the brain area will change accordingly [2]. From the changing signal, a task-related (CTR) brain active zone can be located using a related algorithm. Therefore, how to quickly and accurately locate the active area is of great significance for the corresponding psychological behaviors and diseases.

To address fMRI activation location, many scholars have proposed a variety of algorithms, where Statistical Parametric Maps (SPMs) [3,4] are widely used. SPMs is a statistical method, and convolves a stimulus function corresponding to a task with a Hemodynamic Response Function (HRF) to obtain a general linear model (GLM) [5] design matrix. A restricted maximum likelihood (REML) [6] or Bayesian algorithm [7,8] can be used to estimate the GLM parameters. Under a null hypothesis, then, the GLM parameters statistically analyzed through methods such as T test and F test, so as to obtain the statistical maps of the parameters about brain activation regions. However, this method requires the GLM design matrix [9] to be known in advance, and the matrix design has some uncertainties. Thus, how to design the matrix will directly affect the locating result. In addition, in order to make an fMRI voxel's probability distribution closer to the Gaussian distribution, this method also needs to perform temporal and spatial smoothing [10]. This will degrade the temporal and spatial resolution of fMRI data.

In fact, the observed fMRI signals can be seen as a linear combination of spatial maps (SMs) of activations and time courses (TCs) [11]. Therefore, locating fMRI activations can be regarded as a blind source separation (BSS) [12] issue. Most BBS algorithms use the statistics of observed signals to complete the separation. From this, blind separation algorithms can be roughly divided into higher-order-statistics [13–15] and second-order-statistics algorithms [16]. In higher-order-statistics algorithms, the most widely used one is independent component analysis (ICA) [17–22], which uses maximized kurtosis, likelihood or negative entropy to separate signals that are statistically independent and satisfy non-Gaussian distribution characteristics. The earlier application of ICA to fMRI separation is proposed in [17]. Without the estimation of TC, the method uses Comon's ICA algorithm [18] and Bell's ICA algorithm [19] to achieve an accurate separation of CTR activations. However, the both show slow convergence. In many ICA methods,

* Corresponding author.
E-mail address: whf5469@gmail.com (H. Wu).

https://doi.org/10.1016/j.dsp.2021.103137
1051-2004/

FastICA [20] adopts batch computation and fixed-point iteration and thus has fast convergence and high robustness. GIFT (Group ICA of fMRI Toolbox) method [21] uses FastICA, where multiple subjects are combined into a group to reduce noise and a principal component analysis (PCA) algorithm performs dimensionality reduction [23]. It can effectively find the CTR activations and have better computation speed. Even for the faster FastICA in ICA algorithms, however, its computational complexity is still high due to its fourth-order statistics and much iteration for convergence. Compared with higher-order ICA algorithms, second-order blind identification (SOBI) algorithms [24–26] only calculate a correlation matrix of observed signals. Thus, they are less computationally complex and also receive many attentions. Unfortunately, the fMRI activation signals appear sparsity [27], each of which only has values in its activation regions and are close to zero in the other regions. Therefore, the information that the autocorrelation matrix of the fMRI signals contains is not rich. This will cause that the application of SOBI to fMRI separation will produce more separation errors. In order to solve the difficulty for SOBI to separate sparse signals, a frequency-domain SOBI (f-SOBI) algorithm [28] is proposed. The algorithm performs inverse Fourier transform on the signals to obtain a rich autocorrelation matrix, which can achieve better separation of sparse signals. However, the algorithm has to be performed in the case with small noise. When the noise of the fMRI signal is large, the separation performance of f-SOBI will decrease.

In this paper, we propose an inverse-sparse transformation method to solve the difficulty of second-order blind separation of fMRI signals. The idea of this method is to transform the sparse fMRI signals into another domain, so that the transformed signals no longer have sparsity. Thus, the autocorrelation matrix of the transformed signals contains more information and the observed fMRI signals can be better separated. From the idea, we derive that the transformation matrix of inverse-sparse transformation should be orthogonal, for example, orthogonal wavelet transform, dictionary learning and other orthogonal transformation methods can be [29–31]. From the view of the transformation matrix, the f-SOBI algorithm is only an inverse-sparse algorithm using an orthogonal inverse-Fourier transform matrix. In order to make f-SOBI can be used for the separation of noisy fMRI signals, we perform group-dimension reduction and whitening on the fMRI signals of multiple subjects with same tasks and thereby propose a called group f-SOBI (GFS) algorithm. To further reduce the complexity of GFS, we use an orthogonal cosine transform matrix to perform an inverse-sparse transform, and propose a called group-cosine SOBI (GCS) algorithm. Because GFS and GCS both use second-order statistics, their complexity is lower than that of higher-order ICA algorithms.

In experiments, we use a public simulation software named SimTB [32] to generate a group of simulation data, and also use a group of real fMRI data to test the algorithms. For the simulation data, the separation error of the proposed algorithms is less than half that of traditional SOBI and close to that of ICA, but their running time is only 1/30 of ICA. For the real data, the locations of activations by the proposed algorithms are consistent with ICA, but their running time is only 1/5 of ICA.

2. Localizing FMRI activation method

2.1. SPM method

SPM method [3,4] is a widely used method for localizing fMRI activations. This method generally uses the GLM model. As shown in Fig. 1, let BOLD signals $\mathbf{y} \in \mathbb{R}^{T\times 1}$ be expressed as [5]

$$\mathbf{y} = \mathbf{D}\boldsymbol{\beta} + \mathbf{e} \tag{1}$$

where

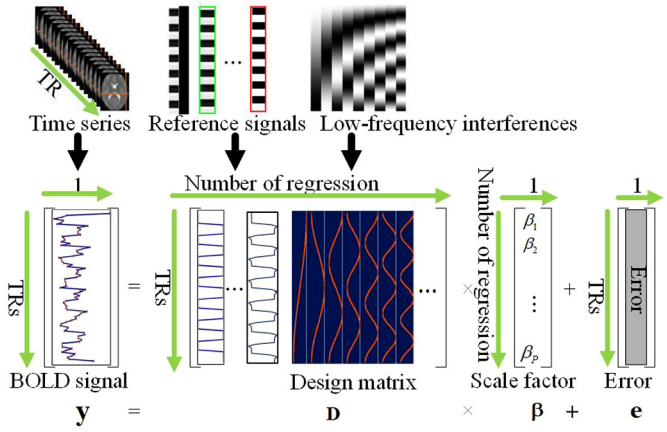

Fig. 1. Generalized linear model in SPM.

T is the number of scans, i.e. a time factor,

$\mathbf{D} \in \mathbb{R}^{T\times P}$ is a design matrix consisting of reference signals and basis functions that can be obtained in experiments,

$\boldsymbol{\beta} \in \mathbb{R}^{P\times 1}$ is a scale coefficient vector of regression,

P is the number of regression coefficients,

$\mathbf{e}$ is an error vector.

Therefore, given the observation $\mathbf{y}$, an objective function $J(\boldsymbol{\beta}|\mathbf{D},\mathbf{y})$ can be designed to obtain an estimation of $\boldsymbol{\beta}$ as $\hat{\boldsymbol{\beta}} = \arg\max_{\boldsymbol{\beta}} J(\boldsymbol{\beta}|\mathbf{D},\mathbf{y})$. Different objective functions will produce different estimation methods, such as constrained maximum likelihood estimation [33], Bayesian estimation [34] and so on. After obtaining $\hat{\boldsymbol{\beta}}$, we can use a null hypothesis $H_0 : \mathbf{c}^{\mathrm{T}}\hat{\boldsymbol{\beta}} = 0$, where $\mathbf{c}$ is a selection vector. When the distribution of the statistic $\bar{T}$ is known, such as a t distribution or a F distribution, then given a significance level α, the threshold can be obtained from

$$\alpha = p(\bar{T} > t_\alpha | H_0) \tag{2}$$

If $t > t_\alpha$ where the statistic t comes from $\mathbf{c}^{\mathrm{T}}\hat{\boldsymbol{\beta}}$, the hypothesis can be rejected and the corresponding regions are activations. From (1) and (2), SPM uses statistical methods to finding activations and it requires the design matrix $\mathbf{D}$ be known so that $\boldsymbol{\beta}$ can be estimated. However, the design of $\mathbf{D}$ involves some uncertain factors such as hemodynamic response function (HRF), exogenous stimuli and low frequency interference. Improper matrix design will affect the final estimation results.

2.2. ICA method

The blind source separation method like ICA does not require a known design matrix. Its linear mixed model can be seen as an extension of GLM model in (1) to multiple voxels, shown in Fig. 2. If the v-th voxel BOLD signal is denoted as $\mathbf{y}_v \in \mathbb{R}^{T\times 1}$, the V voxel signal matrix $\mathbf{Y} = [\mathbf{y}_0, \mathbf{y}_1, \ldots \mathbf{y}_{V-1}] \in \mathbb{R}^{T\times V}$ can be expressed as

$$\mathbf{Y} = \mathbf{AS} + \mathbf{N} \tag{3}$$

where

$\mathbf{A} = [a_{tc}] \in \mathbb{R}^{T\times C}$ is a mixed matrix, i.e. a TC matrix,

$\mathbf{S} = [\mathbf{s}_0, \mathbf{s}_1, \ldots \mathbf{s}_{C-1}]^{\mathrm{T}} \in \mathbb{R}^{C\times V}$ denotes component activation signal,

$\mathbf{N} = [n_{tv}] \in \mathbb{R}^{T\times V}$ denotes additive noise,

C is the number of components.

For the ICA algorithms based on (3), the GIFT algorithm has better separation performance and robustness. First, it performs principal component analysis (PCA) on fMRI signals $\{\mathbf{Y}^{(m)}\}_{m=1}^{M}$ of M subjects who perform the same cognitive task, so that $E\{\mathbf{z}_v\mathbf{z}_v^{\mathrm{H}}\} = \mathbf{I}_{N\times N}$

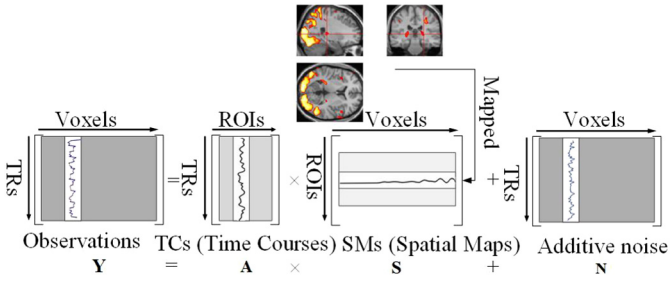

Fig. 2. Linearly mixed model in GIFT.

where $\mathbf{z}_v$ is the v-th column vector of $\mathbf{Z} \in \mathbb{R}^{N\times V}$, $\mathbf{Z}$ is a dimension-reduced and whitened matrix and N is the dimension-reduction number. Then, ICA separation is performed on the whitened signal matrix $\mathbf{Z}$. Taking FastICA with better running speed and robustness as an example, the separation matrix is obtained by

$$\mathbf{W}_{k+1} = E\left\{\mathbf{Z}g\left(\mathbf{W}_k^{\mathrm{T}}\mathbf{Z}\right)\right\} - E\left\{g'\left(\mathbf{W}_k^{\mathrm{T}}\mathbf{Z}\right)\right\}\mathbf{W}_k \tag{4}$$

where $g(\cdot)$ is the derivative of a negative entropy approximation function, $(\cdot)'$ denote a derivative and k is the number of iterations. From (4), FastICA algorithm needs to compute a negative entropy function which is generally a fourth-order statistic, and its separation matrix $\mathbf{W}$ requires many iterations. Therefore, when FastICA is applied to fMRI signal separation, its computational complexity may not be optimal.

2.3. SOBI method

Compared with ICA with higher-order statistics, SOBI [16] only computes the second-order statistics, so the complexity can be reduced much. SOBI first computes the correlation matrix $\mathbf{R}_z(\tau) = E\{\mathbf{z}_{v-\tau}\mathbf{z}_v^{\mathrm{H}}\}$, and then performs eigenvalue decomposition $\mathbf{R}_z(\tau) = \mathbf{U}\mathbf{\Lambda}(\tau)\mathbf{U}^{\mathrm{H}}$ where $\mathbf{\Lambda}(\tau)$ is a diagonal matrix of eigenvalues and $\mathbf{U}$ is a matrix of eigenvectors. Theoretically, the component activation is from $\mathbf{U}^{\mathrm{H}}\mathbf{Z}$. Because the estimation of $\mathbf{R}_z(\tau)$ is sometimes inaccurate, however, the separation is less robust. For this, multiple correlation matrices about τ need to estimated, denoted as $\mathbf{R}_z(\tau_1), \mathbf{R}_z(\tau_2), \ldots \mathbf{R}_z(\tau_p)$. These correlation matrices are jointly diagonalized to obtain the matrix [16]

$$\mathbf{U} = \mathbf{JD}\{\mathbf{R}_z(\tau_1), \mathbf{R}_z(\tau_2), \ldots \mathbf{R}_z(\tau_p)\} \tag{5}$$

where $\mathbf{JD}(\cdot)$ represents the joint diagonalization function. From (5), SOBI's blind separation requires several correlation matrices. If the signal source itself is a sparse signal, the value of the correlation matrix will be very small and the separation matrix will be difficult to be obtained. Unfortunately, the component activation signals are often sparse signals.

2.4. f-SOBI method

For the problem, f-SOBI considers BOLD signals as frequency-domain signals and perform an inverse-Fourier transform on them. Thus, the i-th row and the j-th column factors of the transformation matrix can be expressed as

$$w_{ij}^f = e^{\frac{2\pi \mathrm{i}}{V}ij} \tag{6}$$

Since the transformed signals are not sparse any longer, the separation matrix can be from the correlation matrix of the transformed signals. However, f-SOBI requires less noise in observation signals. Due to various noises in BOLD signals, f-SOBI directly applied to fMRI signal separation is not very good.

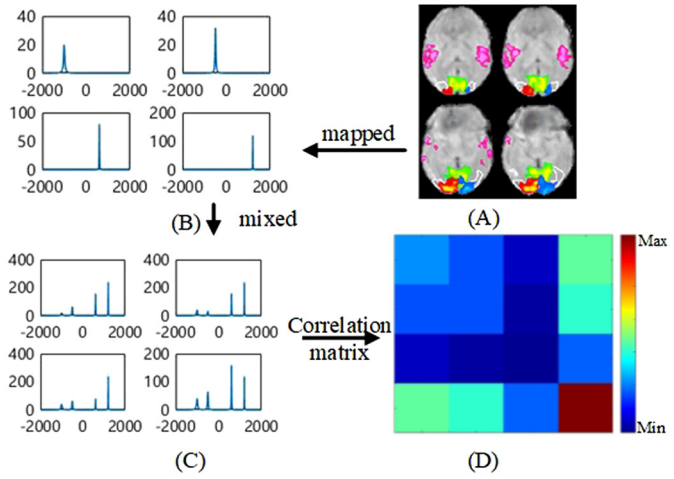

Fig. 3. Correlation matrix of sparse activation signals: (A) brain activation signals, (B) brain activation signals mapped to one-dimension data, (C) Mixed signal, (D) Correlation matrix of mixed signals. (For interpretation of the colors in the figure(s), the reader is referred to the web version of this article.)

3. Sparsity of FMRI signal

The traditional GIFT uses FastICA algorithm to separate fMRI BOLD signals. However, it requires the computation of fourth-order statistics and many iterations and the computational complexity is not optimal. Thus, this paper considers SOBI algorithm with less computational complexity. However, the traditional SOBI algorithm does not consider signal sparsity. From the fMRI linear mixture model in (3), the source signal matrix $\mathbf{S}$ consists of brain component activations, and it will be sparse signals after mapped to one-dimensional signals, as shown in Fig. 3(A) and Fig. 3(B). Even after the signal is mixed with the TC matrix $\mathbf{A}$, the signal $\mathbf{Y}$ is still sparse, as shown in Fig. 3(C). SOBI needs to compute the correlation matrix of the observed fMRI signal $\mathbf{Y}$. Due to the sparsity of $\mathbf{Y}$, the correlation matrix of $\mathbf{Y}$ will contain less information, as shown in Fig. 3(D). Therefore, if we directly apply SOBI to the BOLD signal separation, the performance of the separation will be affected.

This paper will consider a method to transform the mixed sparse signal to an inverse-sparse domain, so that the signal is no longer sparse. And then, the correlate matrix will be obtained from the transformed signals. In this case, the information contained in the correlation matrix will be more than the correlation matrix directly from the sparse signal. Thus, the separation matrix obtained from the correlation matrix will be more accurate.

4. Algorithm

4.1. Separation matrix of inverse-sparse transform

The second-order blind separation algorithm of anti-sparse transform needs to perform inverse-sparse transform on the signals of sparse BOLD signals, and then solve the correlation matrix to obtain the separation matrix. This section will explain how to solve the separation matrix after inverse-sparse transform. Let $\mathcal{F} \in \mathbb{C}^{T\times T}$ be a linear inverse-sparse transform matrix. Performing a linear inverse-sparse transform on each row vector in the dimension-reduction whitened $\mathbf{Z}$ matrix will obtain the matrix

$$\mathbf{X} = \mathbf{Z}\mathcal{F} \tag{7}$$

In this case, we have the following theorem.

Theorem 1. *If the inverse sparse transformation matrix $\mathcal{F}$ is an orthogonal transformation matrix, that is*

$$\mathcal{F}^{\mathrm{H}}\mathcal{F} = \mathcal{F}\mathcal{F}^{\mathrm{H}} = \mathbf{I}$$

we will have

$$\mathbf{U} = \mathbf{JD}\{\mathbf{R}_x(\tau_1), \mathbf{R}_x(\tau_2), \ldots \mathbf{R}_x(\tau_P)\} \tag{8}$$

where $\mathbf{R}_x(\tau) = E(\mathbf{x}_v \mathbf{x}_{v+\tau}^{\mathrm{H}})$, $\tau \in \{\tau_1, \tau_2, \ldots \tau_P\}$, $\mathbf{x}_v$ is the v-th column vector of the matrix $\mathbf{X}$.

Proof. From (7), there is

$$\mathbf{R}_x(\tau) = \lim_{V\to+\infty} \frac{\mathbf{X}\mathbf{X}^{(\tau)\mathrm{H}}}{V} = \lim_{V\to+\infty} \frac{\mathbf{Z}\mathcal{F}(\mathbf{Z}^{(\tau)}\mathcal{F})^{\mathrm{H}}}{V}$$

where $(\bullet)^{(\tau)}$ denotes that a matrix is shifted to the left by τ columns. Since the inverse-sparse transformation matrix $\mathcal{F}$ is a unitary matrix, there are

$$\mathbf{R}_x(\tau) = \mathbf{R}_z(\tau) \tag{9}$$

Substituting (9) into (5) will have (8). □

Theorem 1 shows that as long as the inverse-sparse transformation matrix $\mathcal{F}$ is a orthogonal matrix, the separation matrix can also be obtained by jointly diagonalizing the correlation matrix $\mathbf{R}_x(\tau)$, $\tau = \tau_1, \tau_2, \ldots \tau_P$ after the inverse-sparse transformation. If $\mathbf{X}$ inverse-sparse transformed by $\mathcal{F}$ no longer has a sparse form, the transformed correlation matrix $\mathbf{R}_x(\tau)$ will contain more information than the original correlation matrix $\mathbf{R}_z(\tau)$. Therefore, the separation matrix from the transformed correlation matrix will become more accurate.

4.2. Correlation matrix of anti-sparse transform

To obtain the separation matrix $\mathbf{U}$, we first need to compute the inverse-sparse transformed correlation matrix $\mathbf{R}_x(\tau)$. One of methods is to perform two steps, first performing an inverse-sparse transform and then computing the correlation matrix. However, the computational complexity of this method is not optimal, and computing the correlation matrix in one step will be better.

Let $\mathbf{z}_m = [a_0, a_1, \ldots a_{V-1}]$ and $\mathbf{z}_n = [b_0, b_1, \ldots b_{V-1}]$ be the m-th and n-th row vectors of the matrix $\mathbf{Z}$, and $\mathbf{x}_m = [\alpha_0, \alpha_1, \ldots \alpha_{V-1}]$ and $\mathbf{x}_n = [\beta_0, \beta_1, \ldots \beta_{V-1}]$ be the m-th and n-th row vectors of the matrix $\mathbf{X}$, respectively i.e.

$$\alpha_j = \sum_{i=0}^{V-1} a_i w_{ij}, \quad \beta_{j-\tau} = \sum_{i=0}^{V-1} b_i w_{i,j-\tau} \tag{10}$$

where $\mathcal{F} = [w_{ij}] \in \mathbb{C}^{T\times T}$. Then, we have the following theorem.

Theorem 2. *If the inverse sparse transformation matrix $\mathcal{F}$ is an orthogonal transformation matrix, the m-th row and n-th column element of the matrix $\mathbf{R}_x(\tau)$ can be obtained from*

$$r_{m,n}^x(\tau) = \sum_{i=0}^{V-1} a_i b_i^* \bar{w}_{i\tau} \tag{11}$$

Where

$$\bar{w}_{i\tau} = \sum_{j=0}^{V-1} w_{ij} w_{i,j-\tau}^* \tag{12}$$

Proof. Since

$$r_{m,n}^x(\tau) = \frac{1}{V} \sum_{j=0}^{V-1} \alpha_j \beta_{j-\tau}^* \tag{13}$$

Substituting (10) into (13) will have

$$r_{m,n}^x(\tau) = \frac{1}{V} \sum_{j=0}^{V-1} \sum_{i=0}^{V-1} a_i b_i^* w_{ij} w_{i,j-\tau}^* + \frac{1}{V} \sum_{m=0}^{V-1} \sum_{n=0(n\neq m)}^{V-1} \sum_{j=0}^{V-1} a_m b_n^* w_{mj} w_{n,j-\tau}^* \tag{14}$$

Since $\mathcal{F}$ is a unitary matrix, the second term on the right of (14) is equal to 0. Thus,

$$r_{m,n}^x(\tau) = \frac{1}{V} \sum_{j=0}^{V-1} \sum_{i=0}^{V-1} a_i b_i^* w_{ij} w_{i,j-\tau}^* \tag{15}$$

Substituting (11) into (15), we will have (12). □

Theorem 2 provides another method for solving the correlation matrix $\mathbf{R}_x(\tau)$, which let the sparse signals a_i and b_i multiplied by the transformation factor $\bar{w}_{i\tau}$ and then let them added. Compared with the two-step method of the correlation matrix, the method in Theorem 2 only needs one step.

4.3. Inverse sparse transform matrix

The prerequisite for Theorems 1 and 2 is that the inverse-sparse transformation matrix $\mathcal{F}$ should be an orthogonal transformation matrix. Thus, if the transformation matrix $\mathcal{F}$ is chosen as a Fourier transform matrix, then we will have a so-called f-SOBI algorithm. However, it can be known from (6) that the transformation factor $\exp(ij2\pi \mathrm{i}/V)$ is a complex exponential factor, and the transformation requires multiplication both by the real and imaginary parts of the factor. Since the purpose of the transformation is only to change the sparse signal to non-sparse, we can consider a real transform matrix, an orthogonal cosine transform matrix to reduce the computational complexity. Let $\mathcal{F} = [w_{ij}^c] \in \mathbb{R}^{T\times T}$, where

$$w_{ij}^c = \lambda(j) \cos\left[\frac{\pi(2i+1)j}{2V}\right] \tag{16}$$

$$\lambda(j) = \begin{cases} \sqrt{1/V}, & j = 0 \\ \sqrt{2/V}, & 0 < j < V \end{cases} \tag{17}$$

As can be seen from (16)-(17), the cosine transform can be approximated as only the real part of the inverse Fourier transform. Therefore, the number of multiplications will be reduced by half.

4.4. Algorithm steps and computational complexity

For this fMRI separation algorithm, the transformation matrix needs to be chosen firstly. From Section 4.3, we can use inverse-Fourier or cosine transform matrix. It is noted that the second-order blind separation algorithm should be performed with small noise. Otherwise, the robustness of the joint diagonalization in (8) will not be guaranteed due to the correlation matrix $\mathbf{R}_x(\tau)$ with more errors. Since fMRI signals usually have measurement noise and low-frequency interference, the second-order separation's performance will not be guaranteed. In order to reduce noise and interference, therefore, group PCA dimension-reduction and whitening [22] can be performed on fMRI signals of multiple subjects with the same task. And then, we will compute the correlation

Table 1
Steps of GFS and GCS algorithm.

Input:
fMRI signals of M subjects $\{\mathbf{Y}^{(m)}\}_{m=1}^{M}$;
Output:
Brain activation signal $\hat{\mathbf{S}}$
Known conditions:
Inverse-sparse transform matrix $\mathcal{F} = [w_{ij}] \in \mathbb{C}^{T\times T}$
Steps:
I Dimension reduction whitening pretreatment
① Perform Group PCA on $\{\mathbf{Y}^{(m)}\}_{m=1}^{M}$ such that $E\{\mathbf{z}_v\mathbf{z}_v^{\mathrm{H}}\} = \mathbf{I}_{N\times N}$, where $\mathbf{z}_v$ is the v-th column vector of the matrix $\mathbf{Z} \in \mathbb{R}^{N\times V}$ and N is the dimension reduced
II Correlation matrix calculation
② Perform the inverse Fourier transform or the inverse Cosine transform
③ Compute correlation matrices $\mathbf{R}_x(\tau)$, $\tau \in \{\tau_1, \tau_2, \ldots \tau_P\}$ from (11)
III Signal separation
④ Get the separation matrix $\mathbf{U}$ from (8)
⑤ Get brain activation signal through $\hat{\mathbf{S}} = \mathbf{UZ}$

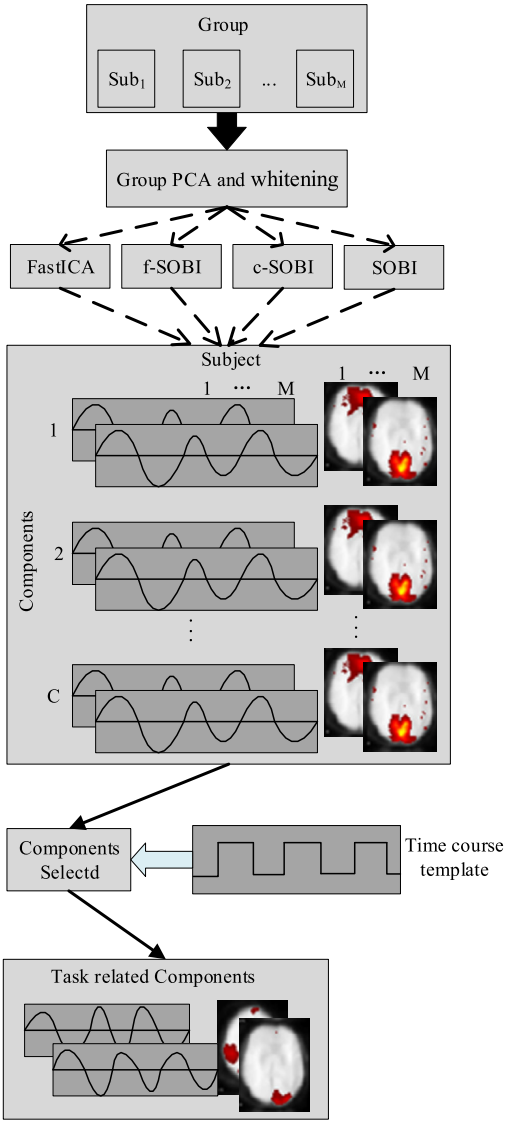

Fig. 4. Algorithm schematic diagram.

matrix and diagonalization. Thus, we will have the corresponding GFS and GCS algorithms, whose steps are shown in Table 1 and Fig. 4.

In addition, Table 2 also shows the complexity of FastICA, SOBI, GFS, and GCS algorithms. Since FastICA computes the fourth-order statistics, it needs $3V$ multiplications. On the other hand, the other four algorithms compute the second-order statistics, so only V multiplications are needed. For the complexity of signal transformation, FastICA and SOBI do not require transformation, so the complexity is not listed in Table 2. When f-SOBI is transformed, it needs multiplications with both the imaginary and real parts of Fourier transformation factors. Assuming that the number of multiplied factors is l_f, the complexity can be expressed as $O(2l_f)$. And, c-SOBI needs multiplications only with the real parts of cosine factors. Thus, the complexity is expressed as $O(l_f)$.

Table 2
The complexity of algorithms.

Algorithm	FastICA	SOBI	GFS	GCS
Complexity of statistics	$O(3V)$	$O(V)$	$O(V)$	$O(V)$
Complexity of transformation	–	–	$O(2l_f)$	$O(l_f)$

Table 3
Some parameters for fMRI simulation data in SimTB.

Experimental parameters	Value
Number of subjects M	3
Number of brain regions C	9
Number of voxels V	21904 (148 × 148)
Number of fMRI scans T	150
Sampling interval TR	2 seconds
CNR1	
Upper limit $\tilde{C}_{\max}$	2
Lower limit $\tilde{C}_{\min}$	0.65
CNR2	
Upper limit $\tilde{C}_{\max}$	5.5
Lower limit $\tilde{C}_{\min}$	5

5. Experiment

5.1. Experimental setup

The experimental data used in this experiment includes simulated data and measured data, which are generated as follows. The simulation data is obtained by SimTB software [32], and its download address is http://trendscenter.org/trends/software/simtb/index.html. Some relevant parameters of the data are given in Table 3. The other parameters are set by a file named by "experiment_params_ aod.m". It should be noted that the fMRI simulation data is assumed to have been aligned, so the D_motion_FLAG parameter is set to 0 in the experiment_params_aod.m file. In addition, we used SimTB software to generate two sets of simulation data with different CNRs, where CNR is defined as

$$CNR = u\left(\tilde{C}_{\max} - \tilde{C}_{\min}\right) + \tilde{C}_{\min} \tag{18}$$

in which u is a random number uniformly distributed between 0-1, $\tilde{C}_{\max}$ represents the upper limit of CNR and $\tilde{C}_{\min}$ represents the lower limit of CNR. Higher CNR means larger signal-to-noise ratio of the data, i.e. smaller noise power. The fMRI measured data is from the public data in GIFT software of TReNDS laboratory [21]. The download address is http://trendscenter.org/trends/software/gift/index.html. Some relevant parameters about the measured data are listed in Table 4 and the other experimental details can be found in [21].

In order to evaluate the performance of the algorithm in this paper, we will give the test results of FastICA, SOBI, GFS and GCS, to separate the above data. The relevant parameters of the algorithms are as follows

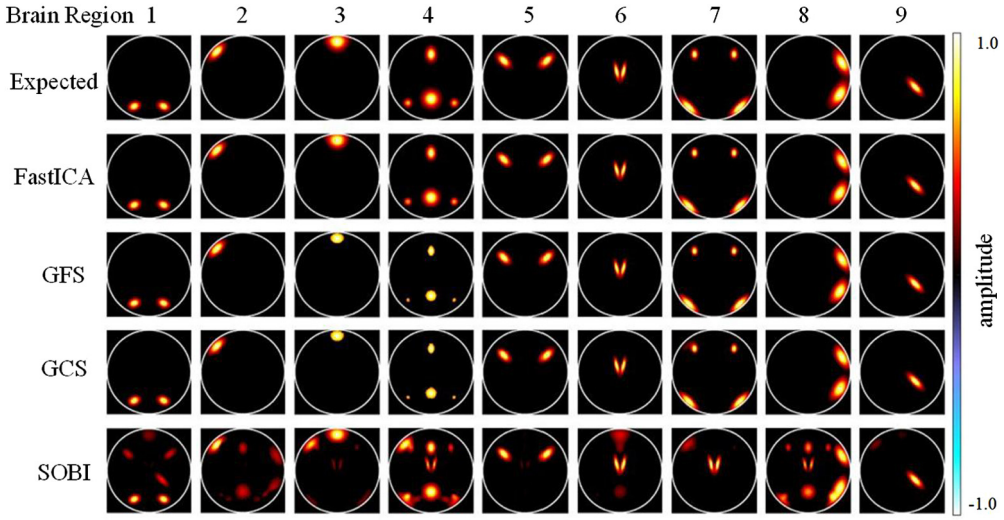

Fig. 5. Separation results for nine simulated brain regions with lower CNR, where the expected brain regions and the regions separated by FastICA, GFS, GCS, and SOBI are given, from top to bottom. All of the brain region signals are normalized to 0-1, and the threshold of the brain regions 3 and 4 separated by GFS and GCS is taken as 0.43 to eliminate the separation noise, i.e. the signals smaller than 0.43 set to 0.

Table 4
Some parameter for fMRI measurement data in TReNDS.

Experimental parameters	Value
Number of subjects M 3	
Number of brain regions C	16
Number of voxels V	50485
Number of fMRI scans T	220

- FastICA: Group PCA algorithm in GIFT software is used for dimension reduction. The number of independent components (IC) is set to 9 and 16 for simulated data and measured data, respectively. Then, the FastICA algorithm of GIFT software is used to separate the signals. The downloaded address is http://trendscenter.org/trends/software/gift/index.html.
- SOBI: Group PCA algorithm is used to reduce the dimensions first. Its parameters are the same as FastICA. The delay τ is set to 1, 2, 3, and 4, respectively.
- GFS: Group PCA and the delay τ value is the same as that of the SOBI. The transformation matrix is from (6).
- GCS: Group PCA and the delay τ value is the same as that of SOBI and the cosine transform matrix is from (16) and (17).

This experiment uses running time to evaluate the computational complexity of each algorithm. In addition, the relative error δ_i and the average error ε are used to evaluate the separation performance of each algorithm, which are defined as:

$$\delta_i = \left(\sum_{j=0}^{V-1} \left| \hat{s}_{ij} - s_{ij} \right| / \sum_{j=0}^{V-1} \left| s_{ij} \right| \right) \times 100\% \quad i = 0, 1, ..C-1 \tag{19}$$

$$\varepsilon = \left(\sum_{i=0}^{C-1} \delta_i \right) / C, \quad i = 0, 1, ..C-1 \tag{20}$$

where $\hat{s}_{ij}$ and s_{ij} are the i-th and j-th elements of the signal matrix $\hat{\mathbf{S}}$ and $\mathbf{S}$, respectively and $\hat{\mathbf{S}}$ are the estimated value of $\mathbf{S}$.

5.2. Simulated data

This section gives the separation results for the data with two kinds of CNRs in Table 3. Fig. 5 shows the result for the simulated fMRI signals with lower CNR, where the expected brain maps and the separated maps by the algorithms are given, respectively. It can be seen from the figure that the brain regions separated by FastICA, GFS, and GCS can correspond to the expected ones. On the other hand, there are noises in brain regions 3, 4, 7, and 8 by SOBI. Especially, the brain region 7 is not consistent with the expected one. The results in Fig. 5 indicate that FastICA, GFS, and GCS have better separation performance than SOBI under lower CNR condition. It is also noted that the regions of some brain activations are smaller than the expected ones, such as the regions 3 and 4 by GFS, but the locations of the strongest signals are consistent.

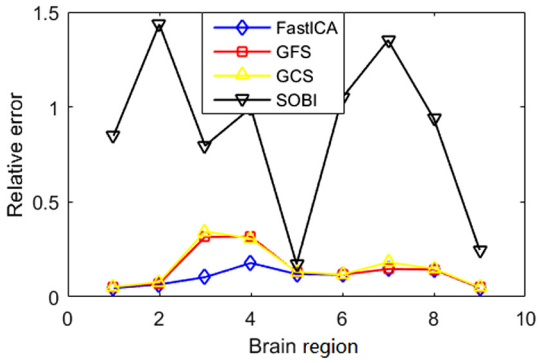

Fig. 6. The separation errors curves for nine simulated brain regions with lower CNR.

Fig. 6 shows the relative error of separated brain regions with lower CNR. As can be seen from Fig. 6, the error curves of SOBI are above the other algorithm curves, while GFS and GCS are between FastICA and SOBI curves. Further, we calculated the average error of the four algorithms. The errors are ranked from small to large as 10% of FastICA, 15% of GFS, 15% of GCS and 85% of SOBI. Although the errors of GCS and GFS are slightly higher than FastICA by 5 percentages, they are much smaller than SOBI by 70 percentages. The results in Fig. 5 show that the separation performance of the proposed algorithm at lower CNR is close to FastICA but much better than SOBI.

Fig. 7 also shows the separated result for the simulated fMRI signals with higher CNR.

Compared with the results in Fig. 5, SOBI has fewer noise in the separated brain regions, and its performance is close to GFS and GCS. Fig. 9 shows the results of the relative separation error with higher CNR. The error of SOBI is also close to GFS and GCS,

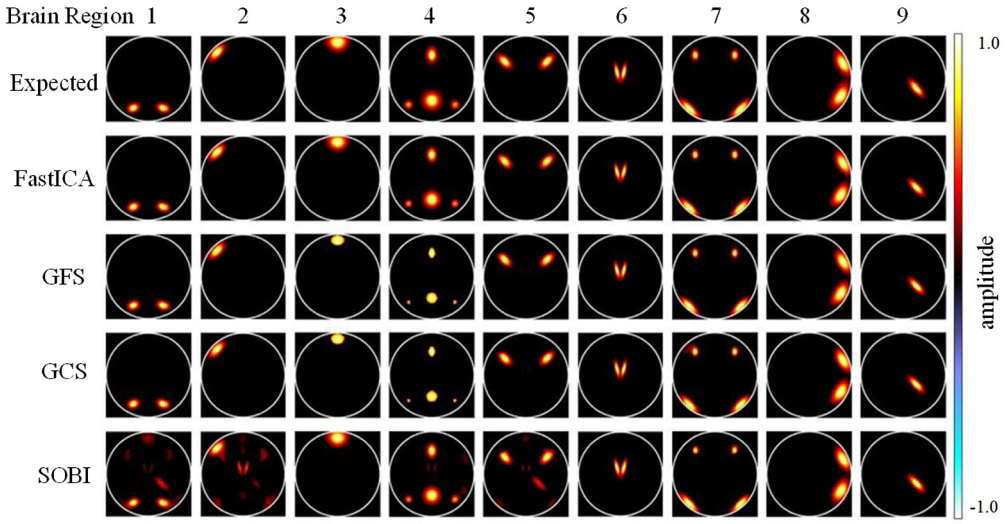

Fig. 7. Separation results for nine simulated brain regions with higher CNR, where the expected brain regions and the regions separated by FastICA, GFS, GCS, and SOBI are given, from top to bottom. All of the brain region signals are also normalized to 0-1, and the threshold of the brain regions 3 and 4 separated by GFS and GCS is also taken as 0.43 to eliminate the separation noise.

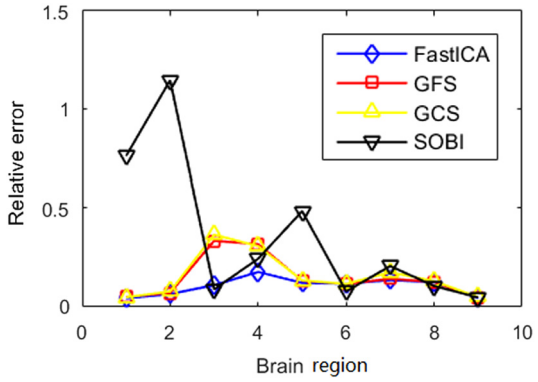

Fig. 8. The separation errors curves for nine simulated brain regions with higher CNR.

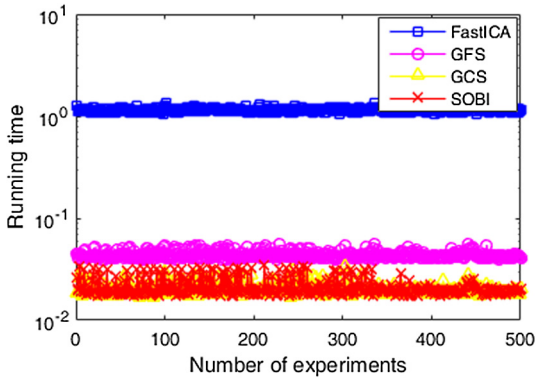

Fig. 9. The running time curves for separation of simulated data. In order to make the running time comparison of the four algorithms more obvious, logarithms were taken in the drawing.

which is consistent with Fig. 7. The results in Fig. 7, Fig. 8 show that under higher CNR conditions, the separation performance of GFS, GCS, and SOBI is close.

Fig. 9 shows the running time for separation of the simulated data. It can be obtained from Fig. 9, the running time ranked from high to low is FastICA, GFS, GCS, and SOBI. Through calculation, the average running time is approximately 1.5, 0.05, 0.02, and 0.02 seconds. It can be seen that the running time of GFS, GCS and SOBI is much shorter than FastICA and less than 1/30 of FastICA. And, the running time of GCS and SOBI is less than half of GFS.

Fig. 10 shows the statistics of the number of multiplications required to execute the four algorithms. It can be seen from the figure that the number of multiplications of FastICA, GFS, GCS and SOBI algorithm is about 4.10 million, 0.18 million, 0.14 million and 0.13 million. The number of repeats of GFS and GCS includes the number of multiplications of statistics and the number of multiplications of transformations. It can be seen that the number of multiplications required to execute the GFS, GCS, and SOBI algorithms is much smaller than that of the FastICA algorithm, while the number of multiplications of the GCS algorithm is slightly higher than that of the SOBI algorithm, but much lower than the GFS algorithm. These results are consistent with the simulated data in Fig. 9.

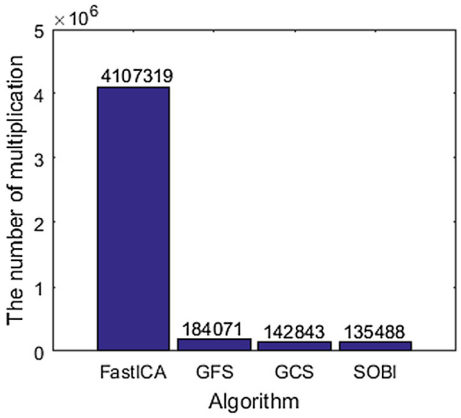

Fig. 10. The number of multiplications performed by the four algorithms.

5.3. Measured data

This sub-section presents the results for the separated brain regions of the measured data given in Table 4. According to literature [21], the fMRI measured data can be separated to 16 more relevant brain regions. Thus, we let the number of components in each algorithm be 16. In order to clearly show the separation results for

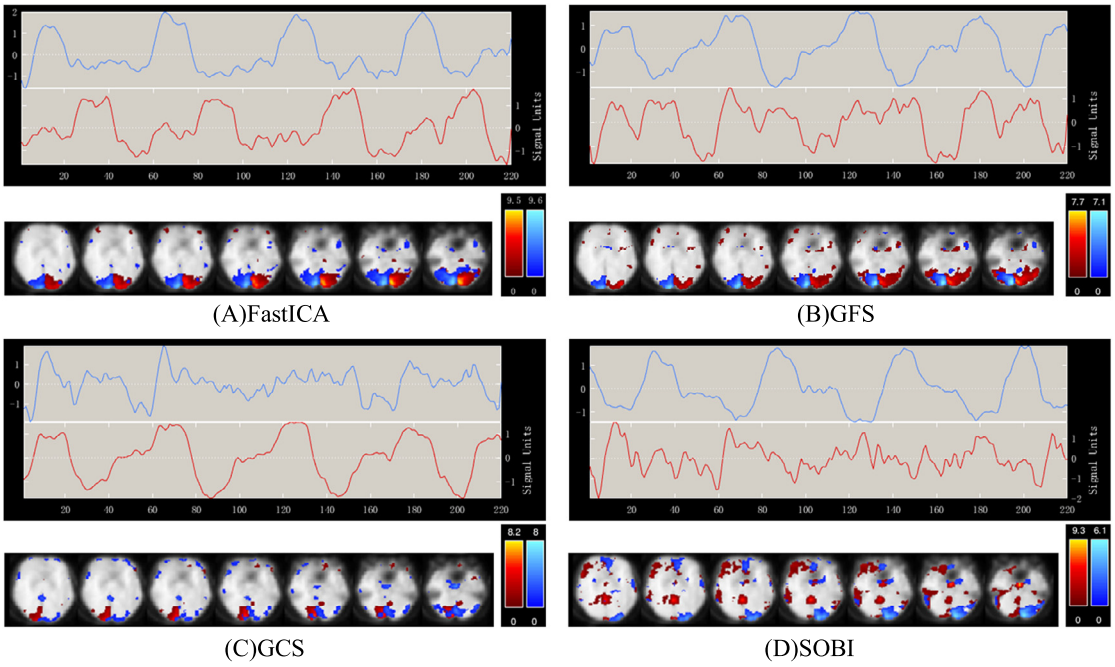

Fig. 11. Brain area results of real data separated by each algorithm, where (A)-(D) correspond to FastICA, GFS, GCS and SOBI algorithms.

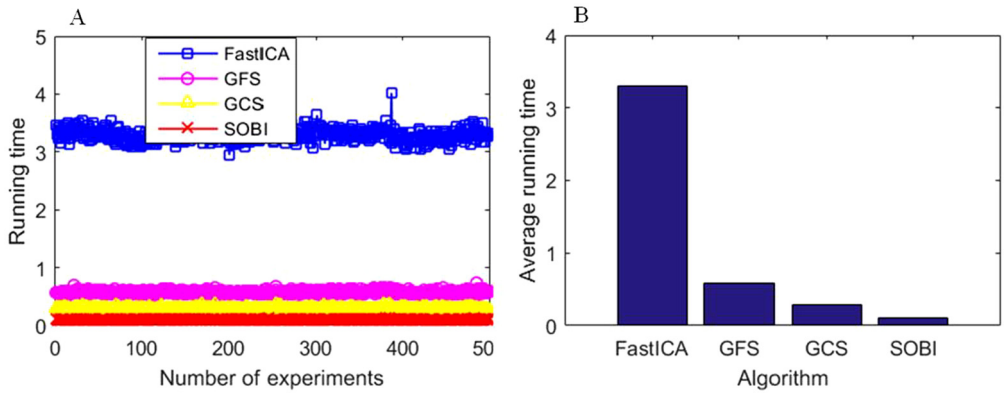

Fig. 12. The running time for separation of measured data, where (A) gives running time curves and (B) gives average running time histograms.

the algorithms, the TC curves about 16 separated brain regions is compared with an exogenous visual stimulation curve in the experiment [21]. And then, we select two separated brain regions with higher correlation, the left and right regions of the primary visual cortex, which are respectively denoted by red and blue in Fig. 11. Also, the TC curves and seven axial slices about the two brain regions are given.

Comparing GFS and GCS with FastICA, we can see that the primary visual cortex separated by GFS and GCS can correspond to that by FastICA. And, there are fewer noises in the regions by GFS and GCS. On the other hand, there are many noisy points for SOBI. Only the right of the primary visual cortex in SOBI can correspond to that in FastICA, and the correspondence of the left area is not obvious. It is also noted that although there is a correspondence among the brain regions by GFS, GCS and FastICA, GCS's region size decreased and GFS does not. The result shows that, the separation performance of GFS is closer to FastICA while SOBI is significantly different from FastICA. The performance from high to low should be FastICA, GFS, GCS, and SOBI.

Fig. 12 gives the running time of the algorithms for the measured data. In Fig. 12(A), the running time curves from high to low are FastICA, GFS, GCS and SOB. The order of the average time in Fig. 12(B) is consistent with Fig. 12(A), about 3.8, 0.8, 0.5, and 0.1 seconds. It can be seen that the running time of GFS, GCS and SOBI is much shorter than FastICA, less than 1/4 of FastICA. And, the running time of GFS, GCS and SOBI is close, but the running time of GCS and SOBI is less than about 2/3 of GFS. These results are consistent with the simulated data in Fig. 11.

6. Discussion

For the blind source separation of fMRI sparse signals, this paper uses inverse Fourier transform and inverse cosine transform to process the signals so that the signals are no longer in sparse form, and then are separated. The experimental results show that compared with the existing FastICA algorithm, the brain activations separated by the proposed method can correspond to those by FastICA while the proposed method's running time is reduced very much. Compared with the existing SOBI algorithm, the proposed method's running time has increased a little, but the separation error can be significantly reduced for the simulated data with low signal-to-noise ratio and the measured data. Although the proposed method displays better performance, the following points need to be discussed further.

For the simulated data, first, the signals separated by FastICA, GFS, GCS, and SOBI all contain positive and negative parts. We only

consider the positive parts as activations. In fact, there are many noises in the separation regions of these three algorithms, but the noises are mainly concentrated in the negative parts. In the experiment, therefore, we take the threshold 0 to remove most of the noises. Besides, some brain regions separated by GFS, GCS, and SOBI are still contains several low-brightness noise points. Taking appropriate thresholds on these brain areas will remove the noise points, e.g. the threshold of 0.43 for regions 3 and 4 in Fig. 5. However, this also causes the brain regions to become smaller. Considering the simulated data with lower CNR3, there still are some noise points in brain regions separated by SOBI when the threshold is set to 0.4. Thus, the threshold is still set to 0.

For the real measured data, this experiment uses the public data in GIFT software package of TReNDS laboratory. Strictly, more databases should be tried to get more convincing results. Since FastICA algorithm select this database to display its performance, the database can give a more intuitive result if we compare the proposed method with FastICA.

7. Conclusion

Traditional fMRI brain region separation uses blind source separation algorithms such as ICA, but this algorithm needs to compute high-order statistics, and the computational complexity is not low. To reduce the computational complexity, this paper proposes an inverse-sparse transform method to achieve the second-order blind separation of fMRI signals, which transforms sparse BOLD signals to an inverse-sparse domain and then compute the autocorrelation matrix to complete the separation. In order to further reduce the computational complexity, we also use a cosine transform to complete a second-order inverse-sparse blind separation algorithm. In the experiments, we test both simulated and measured fMRI data. For the simulated fMRI data, when the noise is larger, i.e. CNR between 0.65 and 2, the separation error of the proposed GFS and GCS algorithms is 5 percentage points higher than FastICA, but the running time is only 1/30 and 1/60 of FastICA. For the measured fMRI data, the brain regions separated by GFS can correspond to those by FastICA. Although the brain regions separated by GCS can correspond to those by FastICA, the region size is reduced. In terms of running time, GFS and GCS is only 1/4 and 1/8 of FastICA.

The code for the GFS and GCS algorithms proposed in this article has been uploaded to GitHub, and its download address is https://github.com/monk5469/GFS_GCS_fMRI.

CRediT authorship contribution statement

Haifeng Wu: Conceptualization, Methodology, Writing - Reviewing and Editing. **Dong Li:** Software, Writing - Original draft preparation. **Mingzhi Lu:** Visualization, Investigation. **Yu Zeng:** Software, Supervision, Validation.

Declaration of competing interest

The authors declare that they have no known competing financial interests or personal relationships that could have appeared to influence the work reported in this paper.

Acknowledgments

This work is supported by the National Natural Science Foundation of China (61762093), the 17th Batch of Young and Middle-aged Leaders in Academic and Technical Reserved Talents Project of Yunnan Province (2014HB019), Program for Innovative Research Team (in Science and Technology) in University of Yunnan Province, the Key Applied and Basic Research Foundation of Yunnan Province (2018FA036), and the Scientific Research Fund project of in Education Department of Yunnan Province (2020Y0238).

References

[1] S.H. Faro, F.B. Mohamed, BOLD fMRI: A Guide to Functional Imaging for Neuroscientists, Springer Science & Business Media, 2010.
[2] N.W. Schuck, Y. Niv, Sequential replay of nonspatial task states in the human hippocampus, Science 364 (6447) (2019).
[3] W.D. Penny, K.J. Friston, J.T. Ashburner, S.J. Kiebel, T.E. Nichols, Statistical Parametric Mapping: The Analysis of Functional Brain Images, Elsevier, 2011.
[4] H. Han, J. Park, Using SPM 12's second-level Bayesian inference procedure for fMRI analysis: practical guidelines for end users, Front. Neuroinform. 12 (2018) 1.
[5] K.J. Friston, et al., Statistical parametric maps in functional imaging: a general linear approach, Hum. Brain Mapp. 2 (4) (1994) 189–210.
[6] A.P. Verbyla, A note on model selection using information criteria for general linear models estimated using REML, Aust. N. Z. J. Stat. 61 (1) (2019) 39–50.
[7] M.N. Tran, N. Nguyen, D. Nott, R. Kohn, Bayesian deep net GLM and GLMM, J. Comput. Graph. Stat. 29 (1) (2020) 97–113.
[8] M. Imani, E.R. Dougherty, U. Braga-Neto, Boolean Kalman filter and smoother under model uncertainty, Automatica 111 (2020) 108609.
[9] J.B. Poline, M. Brett, The general linear model and fMRI: does love last forever?, NeuroImage 62 (2) (2012) 871–880.
[10] K.J. Friston, O. Josephs, E. Zarahn, A.P. Holmes, S. Rouquette, J.B. Poline, To smooth or not to smooth?: bias and efficiency in fmri time-series analysis, NeuroImage 12 (2) (2000) 196–208.
[11] E.A. Allen, et al., A baseline for the multivariate comparison of resting-state networks, Front. Syst. Neurosci. 5 (2011) 2.
[12] X. Hu, et al., Latent source mining in FMRI via restricted Boltzmann machine, Hum. Brain Mapp. 39 (6) (2018) 2368–2380.
[13] A.K. Nandi, Blind Estimation Using Higher-Order Statistics, Springer Science & Business Media, 2013.
[14] C. Chatzichristos, E. Kofidis, M. Morante, S. Theodoridis, Blind fMRI source unmixing via higher-order tensor decompositions, J. Neurosci. Methods 315 (2019) 17–47.
[15] M. Pakravan, M.B. Shamsollahi, Automatic grouping of joint and individual sources, in: Multisubject fMRI Data Using Higher Order Cumulants, IEEE J. Biomed. Health Inform. 23 (2) (2018) 744–757.
[16] A. Belouchrani, K. Abed-Meraim, J.F. Cardoso, E. Moulines, A blind source separation technique using second-order statistics, IEEE Trans. Signal Process. 45 (2) (1997) 434–444.
[17] M.J. McKeown, et al., Analysis of fMRI data by blind separation into independent spatial components, Hum. Brain Mapp. 6 (3) (1998) 160–188.
[18] P. Comon, Independent component analysis, a new concept?, Signal Process. 36 (3) (1994) 287–314.
[19] A.J. Bell, Information theory, independent component analysis, and applications, in: Unsupervised Adaptive Filtering, vol. 1, 2000, pp. 237–264.
[20] A. Hyvarinen, Fast and robust fixed-point algorithms for independent component analysis, IEEE Trans. Neural Netw. 10 (3) (1999) 626–634.
[21] E.B. Erhardt, S. Rachakonda, E.J. Bedrick, E.A. Allen, T. Adali, V.D. Calhoun, Comparison of multi-subject ICA methods for analysis of fMRI data, Hum. Brain Mapp. 32 (12) (2011) 2075–2095.
[22] C. Liu, J. JaJa, L. Pessoa LEICA, Laplacian eigenmaps for group ICA decomposition of fMRI data, NeuroImage 169 (2018) 363–373.
[23] E. SanJuan, et al., Comparison between FastICA and InfoMax for the blind separation of audio signals, in: 2018 11th International Symposium on Communication Systems. Networks & Digital Signal Processing (CSNDSP), IEEE, 2018, pp. 1–4.
[24] F.J. Theis, A. Meyer-Baese, E.W. Lang, Second-order blind source separation based on multi-dimensional autocovariances, in: International Conference on Independent Component Analysis and Signal Separation, Springer, Berlin, Heidelberg, 2004, pp. 726–733.
[25] J. Virta, K. Nordhausen, Blind source separation of tensor-valued time series, Signal Process. 141 (2017) 204–216.
[26] K. Tachikawa, S. Izawa, Y. Ono, A. Ishiyama, Evaluation of performance to detect default mode network among some algorithms applied to resting-state fMRI data, in: 2015 37th Annual International Conference of the IEEE Engineering in Medicine and Biology Society (EMBC), IEEE, 2015, pp. 1805–1808.
[27] Q. Long, S. Bhinge, Y. Levin-Schwartz, Z. Boukouvalas, V.D. Calhoun, T. Adalı, The role of diversity in data-driven analysis of multi-subject fMRI data: comparison of approaches based on independence and sparsity using global performance metrics, Hum. Brain Mapp. 40 (2) (2019) 489–504.
[28] D. Nuzillard, J.M. Nuzillard, Second-order blind source separation in the Fourier space of data, Signal Process. 83 (3) (2003) 627–631.
[29] Y. Zhou, J. Han, X. Yuan, Z. Wei, R. Hong, Inverse sparse group lasso model for robust object tracking, IEEE Trans. Multimed. 19 (8) (2017) 1798–1810.
[30] Y. Yi, Y. Cheng, C. Xu, Visual tracking based on hierarchical framework and sparse representation, Multimed. Tools Appl. 77 (13) (2018) 16267–16289.
[31] J. Mairal, Sparse coding for machine learning, image processing and computer vision, Ecole normale supérieure, Cachan, 2010.
[32] E.B. Erhardt, E.A. Allen, Y. Wei, T. Eichele, V.D. Calhoun, SimTB, a simulation toolbox for fMRI data under a model of spatiotemporal separability, NeuroImage 59 (4) (2012) 4160–4167.

[33] K.J. Friston, K.E. Stephan, T.E. Lund, A. Morcom, S. Kiebel, Mixed-effects and fMRI studies, NeuroImage 24 (1) (2005) 244–252.
[34] K.J. Friston, Bayesian estimation of dynamical systems: an application to Fmri, NeuroImage 16 (2) (2002) 513–530.

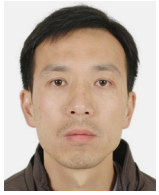

Haifeng Wu received the M.S. degree in electrical engineering from Yunnan University, Kunming, China, in 2004, and the Ph.D. degree in electrical engineering from Sun Yat-Sen University, Guangzhou, China, in 2007. He is currently an professor at the Department of Information Engineering at the Yunnan Minzu University. Prior to that, he was postdoctoral scholar at the Kunchuan Institute of Technology from 2007 to 2009. His research interests include machine learning, neural signal processing and mobile communications.

Dong Li is now pursuing the M.S. degree in electrical engineering from Yunnan Minzu University, Kunming, China. His interests include neural system and machine learning.

Mingzhi Lu received the M.S. degree in electrical engineering from Yunnan Minzu University, Kunming, China. His interests include neural system and machine learning.

Yu Zeng received the M.S. degree in electrical engineering from Yunnan University, Kunming, China, in 2006. She is currently an assistant professor at the Department of Information Engineering at the Yunnan Minzu University. Prior to that, she was an electrical engineer in Kunming Institute of Physics from 2006 to 2009. Her research interests include wireless network and mobile communications.